Narrow-Bandgap Nb2O5 Nanowires with Enclosed Pores as High-Performance Photocatalyst

Journal:	*SCIENCE CHINA Materials*
Manuscript ID	SCMs-2018-0192.R1
Manuscript Type:	Article
Date Submitted by the Author:	31-May-2018
Complete List of Authors:	Zhang, Ying Zhao, Hu Zhao, Xiaofei Lin, Jiannan Li, Na Huo, Ziyang; Queensland Micro- and Nanotechnology Centre, Griffith University Yan, Zifeng Zhang, Miao; University of California Berkeley, Chemistry Hu, Shi
Keywords:	Niobium oxide, photocatalysis, nanowires
Speciality:	nanomaterial synthesis, inorganic synthesis

SCIENCE CHINA Materials ARTICLES

mater.scichina.com link.springer.com

Narrow-Bandgap Nb_2O_5 Nanowires with Enclosed Pores as High-Performance Photocatalyst

Ying Zhang,[1] Hu Zhao,[1] Xiaofei Zhao,[1] Jiannan Lin,[2] Na Li,[2] Ziyang Huo,[3] Zifeng Yan,[1] Miao Zhang[4*] and Shi Hu[2*]

ABSTRACT Niobium oxide nanowires with enclosed pore structure were synthesized via a solvothermal method, which exhibited decreased bandgap, enhanced light absorption and reduced charge-recombination rate. The porous Nb_2O_5 nanowires showed increased performance in the photocatalytic H_2 evolution and photodegradation of rhodamine B, as compared to their nonporous counterparts, which could be ascribed to the peculiar porous nanostructure.

Keywords: Niobium oxide, nanowires, photocatalysis

INTRODUCTION

Niobium (V) oxide (Nb_2O_5) is an important n-type transition metal oxide semiconductor with a bandgap of 3.4 eV, similar to TiO_2 (3.2 eV), which has been demonstrated as a promising materials in gas sensing, electrochromics, acid catalysis, field emission displays, batteries, solar cells and other electronic devices such as memristors[1-7]. In particlar, nanostructured Nb_2O_5 offers high surface to volume ratios and quantum confinement effects that enable unique physical and chemical interactions to occur at the surface[8-10]. As a result, such morphological manipulations significantly influence the optical and electronic properties of Nb_2O_5. However, there are few studies concerning the use of Nb_2O_5 for photocatalytic applications which can be attributed to two intrinsic drawbacks: the wide bandgap (c.a. 3.4 eV), which limits its application to the visible region and the fast recombination rate of photogenerated electron-hole pairs (e−/h+), which reduces the quantum efficiency of the photo-induced redox reaction. A recent study of reduced Nb_2O_5 nanorods demonstrates enhanced light absorption, improved charge separation and transport capability and photocatalytic performance, thanks to the presence of substantial Nb^{4+} cations and oxygen vacancies[11].

Studies have shown that 1D nanostructured photocatalysts provide a continuous long carrier transfer path and can be separated and recycled easily because of their large aspect ratio.[12-14] Among the many varieties of 1D nanostructures, porous nanowires are particularly interesting, not only for the unique porous structural and physical chemical properties, but also for their outstanding performance in optic and electronic fields.[15-23] So far, many groups have reported the growth of the porous 1D semiconductor nanostructures and studied their exceptional performance, such as porous ZnO nanowires with superior photocatalytic activity[24], CdS nanosponges showing high activity for RhB photo-degradation under visible light due to the accessibility of both inner and outer surfaces through the pores in the walls[25], porous TiO_2 nanotubes with improved photocatalytic efficiency due to their larger specific surface areas[26], porous In_2O_3 nanowires with excellent gas sensing properties to H_2S benefiting from surface adsorption and the sulfuration[27], porous SnO_2 nanowire bundles consisting of interconnected nano-crystallites with a remarkable photocatalytic effect for the degradation of RhB and a high de-lithiation capacity[15], and porous Co_3O_4 nanowires with high sensitivity to carbon monoxide because porous structure increases the surface reactive sites and facilitates the diffusion of target gases[28]. These advantages come from the effective diffusion and adsorption of reactant in the porous nanostructures. Porous nanostructures can also induce a change in electronic structures of materials and bring about benefits. For instance, Wan et al. synthesized porous Ag_3PO_4 nanotubes which exhibit higher photocatalytic activity than that of irregular Ag_3PO_4 powder, thanks to the reduced band gap of 2.47 eV and enhanced UV-Vis absorbance[29].

Different from all these reports of porous nanostructures, we report herein our recent discovery on pseudo-hexagonal TT Nb_2O_5 nanowires with an enclosed porous structure which show enhanced pho-

[1] State Key Laboratory for Heavy Oil Processing, PetroChina, Key Laboratory of Catalysis, China University of Petroleum, Qingdao 266580, China
[2] Department of Chemistry, School of Science, Tianjin Key Laboratory of Molecular Optoelectronic Science, Tianjin University, Tianjin 300072, China.
[3] Queensland Micro- and Nanotechnology Centre, Griffith University, Brisbane 4111, Australia
[4] Chemical Science Division, Department of Chemistry, University of California Berkeley 94720, USA
* Corresponding author (email: rychushi@gmail.com, MZhang@lbl.gov)

tocatalytic activity over their nonporous nanowire counterparts for the decomposition of Rhodamine B (RhB) in aqueous solution. We also reveal that a red shift of the absorption edge between nonporous Nb_2O_5 nanowires and porous nanowires annealed at appropriate temperature bring about the bandgap decrease from 3.22 eV to 2.95 eV, and it changed the pathway of RhB degradation and significantly enhanced the photocatalytic H_2 evolution from the water.

EXPERIMENTAL SECTION

Solvothermal synthesis of porous Nb_2O_5 nanowires pNW-580

In a typical synthesis, ammonium niobate (V) oxalate hydrate (9.57 mmol) and oleic acid (2 mL, 90%, Aldrich) was mixed with trioctylamine (13 ml, 98%, Aldrich) in a three-necked round bottom flask with vigorous stirring for 12 h and sonication for 20 min. The mixture was transferred into a 45-ml Teflon-lined autoclave and then heated at 453 K for 6 h. The white precipitates were filtered off, washed several times with ethanol and water, and dried at 353 K for several hours. The dried precipitate was then calcinated at 580 ℃ for 1 h, and collected. The samples calcinated at 400 ℃, 600 ℃and 700 ℃ are also included for comparison and denoted similarly. For instance, pNW-600 stands for the sample annealed at 600 ℃.

Hydrothermal synthesis of nonporous Nb_2O_5 nanowires npNW

The nonporous Nb_2O_5 nanowires were synthesized through a simple hydrothermal method using Nb metal powder and urea as starting materials. In a typical synthesis, Niobium powder (0.122 g) was put into a 65ml urea solution (1-2 M), and then the mixture was transferred into a 100-ml Teflon-lined autoclave and heated at 453K for 4-7 days. Then the white precipitate was collected by centrifugation and washed several times with ethanol and water. Nonporous Nb2O5 nanowires were obtained by calcination of the dried precipitate at 500 ℃ for 2h.

Characterization

Powder X-ray diffraction (XRD) patterns were recorded on a PANalytical X-ray diffractometer by using Cu Ka radiation (λ=0.154 nm, 40 kV/40 mA). Transmission electron microscopy (TEM) images were collected on a JEM-2100 operated at an accelerating voltage of 200 kV. Field emission scanning electron microscopy (FESEM) images were taken using a Hitachi S-4800 scanning electron microscope. Diffuse reflection spectra were recorded on a UV-Vis-NIR spectrometer (Analytik jena; SPECORD plus210) and were converted from reflection to absorbance by the Kubelka-Munk method. The photoluminescence (PL) spectra of the as-synthesized samples in the powder form were investigated at room temperature on a Fluoromax-4 fluorescence spectrophotometer (Horiba Jobin Yvon Japan) with an excitation wavelength (λex) of 325 nm and the width of the excitation and emission slit were 5 and 2 nm, respectively. The emission spectrum was monitored over a wavelength range of 360−600 nm.

Photocatalytic tests

The photocatalytic activity of the samples (porous Nb_2O_5 nanowires and nonporous Nb_2O_5 nanowires) for hydrogen evolution was evaluated in a closed gas circulation and evacuation system under visible light illumination ($\lambda > 420$ nm). Typically, 0.020 g of powder sample was dispersed in 60 mL aqueous solution containing 0.25 M Na_2S and 0.35 M $Na2_SO_3$ in a Pyrex reaction cell. The light source was a 500-W Xe lamp supplying the full wavelength illumination. The amount of produced hydrogen was analyzed with on-line gas chromatograph (GC7900, thermal conductivity detector, high-purity nitrogen as carrier gas).

The photocatalytic activity of the samples (porous Nb_2O_5 nanowires and nonporous Nb_2O_5 nanowires) in degradation of RhB was evaluated in aqueous solution. Typically, 50 mg of photocatalyst was added into 50 mL aqueous solution of RhB (5 mg/l) in a reactor with sonication. The solution was continuously stirred for 1 h in the dark to ensure the establishment of adsorption-desorption equilibrium between the photocatalyst and RhB before irradiation.

Then the solution was illuminated by a 250-W high- pressure mercury lamp with wavelength centred at 365 nm. During the degradation, the RhB solution containing photocatalyst was continuously stirred by a dynamoelectric stirrer and the concentration of RhB was monitored with a SPECORD 210 PLUS UV-Vis spectrometer (Jena).

RESULTS AND DISCUSSION

Powder X-ray diffraction was used to characterize the structure of the as-prepared samples, as shown in Fig 1a. The reflection peaks of porous nanowires pNW-580 and nanonporous nanowires npNW can be well indexed to the pseudo-hexagonal TT phase of Nb_2O_5 (JCPDS number 28-0317), with lattice constants of a = 3.607 Å and c = 3.925 Å. Interestingly, the porous nanowires pNW-580 show a better crystallinity than the nonporous nanowires npNW. The SEM images as shown in Fig. S1 and the TEM images in Fig. 1b and 1c reveal the morphology and structure of the porous and nonporous nanowires respectively. While the nonporous NWs are typically longer than 5 μm and show ripple-like contrast in TEM due to bending-induced strain, the porous NWs pNW-580 are typically shorter than 1 μm and featured with well-separated pores inside the nanowires. The diameter of the pores falls into the range of 5-10 nm and the pores do not move towards the surface of nanowires in the TEM image after large-angle rotation of

SCIENCE CHINA Materials ARTICLES

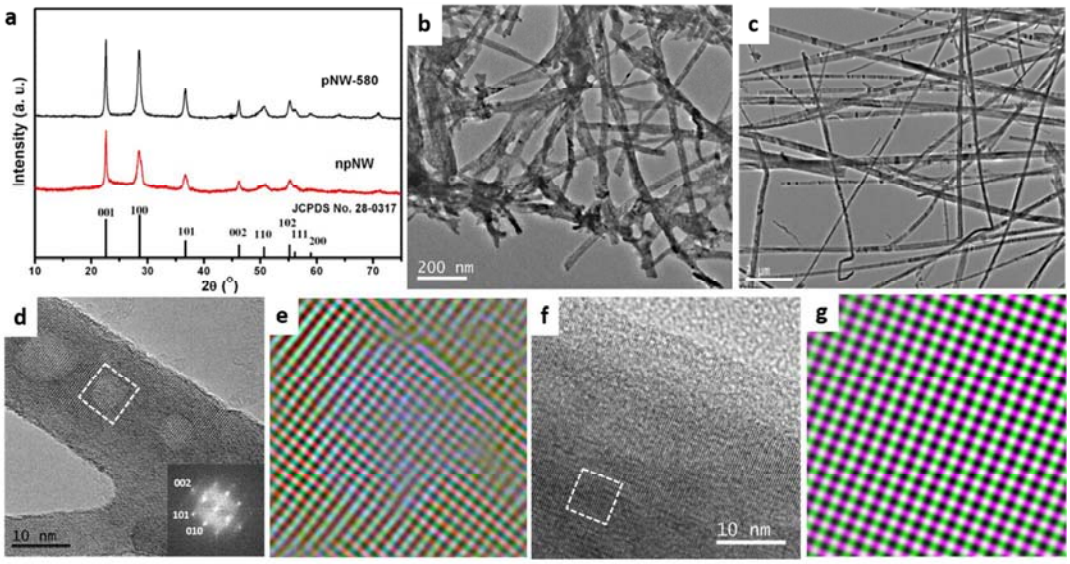

Fig. 1 (a) XRD pattern of the porous nanowires pNW-580 and nonporous nanowires npNW; TEM images of (b) the porous nanowires pNW-580 and (c) nonporous nanowires npNW. HRTEM images of the (d) porous nanowires pNW-580 and (f) nonporous nanowires npNW with (e) and (g) as constructed inverse FFT images from the selected areas (d) and (f). Inset of (d) shows the electron diffraction pattern of the pNW-580.

the TEM holder, which indicates that all the pores are fully trapped within the nanowires. HRTEM image of the nanowires in Fig. 1d and the Fast Fourier transformation (FFT) pattern in the inset show that all the porous nanowires are single crystalline and oriented along c-axis. The clear lattice fringes perpendicular to growth direction of the nanowires show a spacing of 3.97 Å, corresponding to the (001) crystal planes of pseudo-hexagonal Nb_2O_5. The reconstructed crystal lattice based on the FFT pattern obtained from the porous area (Fig. 1e) shows that the lattice surrounding the pores are severely twisted. On the contrary, the nonporous Nb_2O_5 nanowires show solid structure and non-twisted lattice fringes separated by 3.97 Å with the same growth direction along c-axis, as shown in the HRTEM of Fig. 1f and reconstructed crystal lattice of Fig. 1g. The annealing temperature after solvothermal treatment has a significant impact on the morphology and phase stability of the porous nanowires. As shown in the TEM image of Fig. S2, the porosity of pNW-600 is much higher than pNW-580 while the crystallinity of pNW-600 apparently decreases. In addition, increased annealing temperature causes the gradual formation of orthorhombic phase in pNW-600 and pNW-700 while pNW-580 is pristine TT-phase, as is shown in Fig. S3.

The formation of enclosed-pore structure was generally considered as a result of ligand assembly process. The ligands of OA and TOA replaced the oxalate anion and coordinated with the Nb center as structure directing agent at an elevated temperature. Hydrophobic interactions between methylene chains of the TOA and OA molecules in 3D space leads to self-assembly structure with hydrophobic core and surrounding Nb species. After removing the organic template by calcination at 853 K, the cores transform into pores and the coordination structure form crystalline porous nanowires of Nb_2O_5.

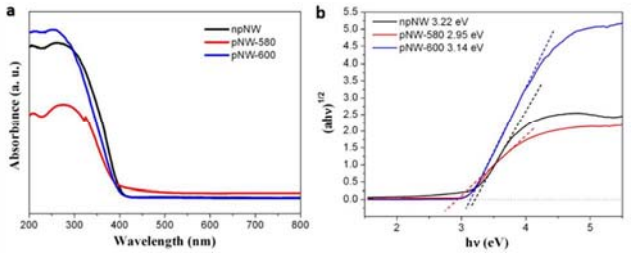

Fig. 2 (a) Diffuse Reflectance spectrum and (b) plots of $(ahv)^{1/2}$ vs photon energy (hv) of the porous pNW-580, pNW-600 and nonporous Nb_2O_5 nanowires pNW with the absorption edge indicated in the legend of (b).

Diffuse reflectance UV–visible spectroscopy was employed to study the optical properties of the porous

[1] State Key Laboratory for Heavy Oil Processing, PetroChina, Key Laboratory of Catalysis, China University of Petroleum, Qingdao 266580, China
[2] Department of Chemistry, School of Science, Tianjin Key Laboratory of Molecular Optoelectronic Science, Tianjin University, Tianjin 300072, China.
[3] Queensland Micro- and Nanotechnology Centre, Griffith University, Brisbane 4111, Australia
[4] Chemical Science Division, Department of Chemistry, University of California Berkeley 94720, USA
* Corresponding author (email: rychushi@gmail.com, MZhang@lbl.gov)

nanowires pNW-580, pNW-600 and the nonporous nanowires npNW, as shown in Fig. 2a. The absorption spectrum of the pNW-580 shows a sharp absorption edge at 2.95 eV or 420 nm, deduced by extrapolation of the linear part of the rising absorption curve, which is red-shifted from the edge of the nonporous nanowires at 3.22 eV or 385 nm (Fig. 2b). The decreased band gap of pNW-580 can be accounted for by the mid-gap states formed by the under-coordinated ions in the twisted lattice surrounding the pores. These results clearly revealed that lower bandgap of pNW-580 could be attributed to the unique enclosed porous structure. However, the pore structure does not necessarily bring about mid-gap states and decreased bandgap, as can be found in the case of pNW-600. The absorption edge of pNW-600 falls at 3.14 eV, which is significantly upshifted from pNW-580 and close to npNW. It is possibly due to the reconfiguration of the under-coordinated atoms around the pores through annealling at higher temperature during which the phase transition from pheudo TT to orthorhombic Nb_2O_5 occurs. The mid-gap states are also removed through this process. Comparison of the Raman spectra of the different nanowires (Fig. S4) indicates the decreasing bond order of the Nb-O polyhedra and disordered structure in porous nanowires of pNW-580 which can be attributed to the increased oxygen vacancies[30].

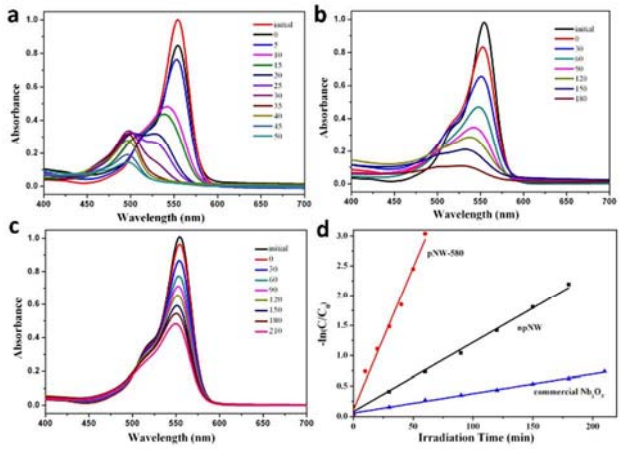

Fig. 3 The UV-Vis spectra of RhB photo-degradation by (a) porous Nb_2O_5 nanowires, (b) nonporous Nb_2O_5 nanowires and (c) commercial Nb_2O_5 under UV irradiation, (d) the photo-degradation rate curve of the samples of porous Nb_2O_5 nanowires, nonporous Nb_2O_5 nanowires and commercial Nb_2O_5.

Since the band gap of the porous nanowires pNW-580 falls into the visible range, they could be considered as a potential candidate for high-performance photocatalysts. They were first evaluated in the photocatalytic degradation of RhB in aqueous solution under ultraviolet irradiation and compared to the performance of nonporous Nb_2O_5 nanowires. As shown in Fig. 3a, the maximum absorption of the RhB solution exhibited significant hypsochromic shifts under ultraviolet irradiation in the presence of porous Nb_2O_5 nanowires. The shift of maximum wavelength from 556 to 498 nm was completed after irradiation for 50 min, which corresponds to the N-deethylation of RhB in the photocatalytic degradation[31]. However, in the presence of nonporous nanowires of Nb_2O_5, the characteristic absorption of RhB around 556 nm decreased to about zero within 180 min, in a mineralization process with no wavelength shift for the maximum absorption of the solution during the whole degradation process (Fig. 3b). Similar mineralization degradation of RhB under UV light irradiation was observed when commercial Nb_2O_5 and pNW-600 were used, but with a much slower reaction rate, as shown in Fig. 3c and Fig. S5.

A pseudo-first-order equation was applied to describe the kinetic data for the as-prepared samples and commercial Nb_2O_5, as is shown in Fig. 3d. The apparent rate constant was calculated to be k=0.047 min^{-1} for the porous nanowires, k=0.011 min^{-1} for the nonporous nanowires and k=0.0032 min^{-1} for the commercial sample. The rate constant of the porous Nb_2O_5 nanowires is 4 times that of the nonporous nanowires, and 15 times that of commercial Nb_2O_5, demonstrating the excellent photo-degradation capability of the porous nanowires.

To further investigate the photo-catalytic activity of the porous nanowires, we evaluated their performance the photo-degradation of RhB under visible light (λ>420 nm) irradiation. As shown in Fig. S6, the visible-light induced photo-decomposition of the RhB in the presence of pNW-580 was significant with 90% of RhB decomposed after 60 min of visible light irradiation. In addition, similar characteristics of maximum absorption shift were observed between UV–light and visible-light photolysis according to the light absorption measurement.

The N-deethylation of the fully N, N, N', N'-tetraethylated rhodamine species by OH radicals is mainly a surface reaction on the photocatalysts[32, 33]. In our case, different UV-Vis degradation spectra of RhB (Fig. 3) suggest that the degradation of RhB was dominated through different degradation pathways in the presence of different Nb_2O_5 photocatalysts. The mineralization pathway of RhB indicates that OH radicals are dominating the oxidation reactions, while the N-deethylation of RhB indicates the direct oxidation of dye molecules by the valence band holes[33]. The valence band potential of regular Nb_2O_5 materials at 2.7 V (vs NHE), is more positive than the OH/H_2O redox potential (2.38 V vs NHE).[2] So the photo-generated holes on the valence band of regular Nb_2O_5 materials are able to oxidize the water molecules to produce free OH radicals and the free OH radicals will dominate the oxidation of dye molecules and lead to the mineralization of the RhB. Compared to regular Nb_2O_5 materials, the porous Nb_2O_5 nanowire material has a much nar-

rower bandgap, which shifts from 3.28 eV to 2.88 eV. As shown in the XPS valence-band spectra of the porous and nonporous nanowires of Nb_2O_5 in Fig. S7, the porous nanowires exhibit a valence-band-maximum 2.87 eV below the Fermi level while the nonporous ones 3.08 eV below. Assuming the relatively constant Fermi level, we can conclude with a 0.21 eV upward shift of the valence band maximum. This is in reasonable agreement with the bandgap shrink of 0.3 eV and indicates change of the dye-oxidation pathway. With the shrink of the band gap, the valence band potential of the porous Nb_2O_5 pNW-580 became more negative than the redox potential of the OH/H_2O redox couple. Thus the holes on the valence band of porous Nb_2O_5 nanowires are not able to oxidize water to form OH radicals. And the adsorbed dye molecules on the catalyst surface will be oxidized by the holes as the primary reaction pathway, which results in the N-deethylation product as the main degradation product.

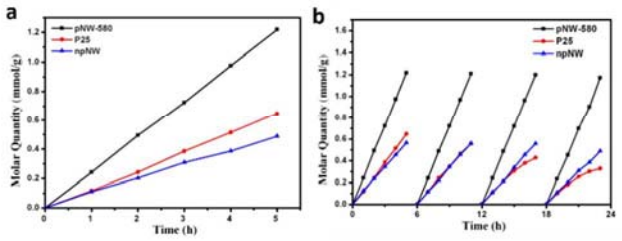

Fig. 4 (a) Photocatalytic H_2 production efficiency of porous Nb_2O_5 nanowires pNW-580, nonporous Nb_2O_5 nanowires npNW and P25, (b) Results of reusability experiments for photocatalytic H_2 generation using the three photocatalysts.

The photocatalytic performance of the porous Nb_2O_5 nanowires was further evaluated in hydrogen evolution reaction and compared with nonporous Nb_2O_5 nanowires and P25, as shown in Fig. 4a. It is clear that the hydrogen evolution rate of the porous Nb_2O_5 nanowires pNW-580 (243.8 μmol g^{-1} h^{-1}) is much higher than that of nonporous nanowires npNW (ca. 113.1 μmol g^{-1} h^{-1}) and P25 powder (ca. 129.6 μmol g^{-1} h^{-1}), suggesting that the creation of pores in the nanowires significantly improves the photocatalytic activity for H_2 evolution. To further evaluate their catalytic stability, all the photocatalysts were recovered and reused for photocatalytic H_2 production under the same conditions. As shown in Fig. 4b, there is nearly no loss of hydrogen evolution rate for both porous and nonporous nanowire photocatalysts, whereas the catalytic activity of P25 evidently declined after 3 cycles. This confirms that the obtained porous Nb_2O_5 nanowires are much more stable than the commercial product P25 while maintaining a higher photocatalytic activity.

All in all, the photocatalytic properties of oxides strongly depend on the band gap, crystallinity and surface area. Generally, large surface area enhances the physical adsorption of reactants and the dispersibility of the powdered photocatalysts. However, the measured BET surface area for the porous and nonporous nanowires is 38.2 and 37 m^2 g^{-1} respectively and with similar pore-size distribution (Fig. S8). The negligible difference in this value implies that surface structure and electronic properties, rather than surface area, are the key factors for the observed difference in catalytic performance of porous and nonporous nanowires. The high performance of porous nanowires pNW-580 is significantly attributed to the improved light absorption due to their decreased band gap. As shown in Fig. 2a, the porous Nb_2O_5 nanowires of pNW-580 show an obvious redshift of 35 nm in the absorption edge, as compared to the nonporous nanowires of npNW. In addition, high crystallinity promotes the efficient transfer of photo-generated carriers from bulk to surface by the suppression of charge recombination process. The crystallinity of the pNW-580 is significantly higher than that of the npNW as shown in the XRD results, in spite of the disturbance of the crystal lattice by the introduction of nanopores. Moreover, the pores inside the nanowires possess a large interfacial region and rich structure defects like the oxygen vacancies and under-coordinated Nb, which can trap the photo-generated electrons, decrease the direct electron-hole recombination and improve the charge carrier separation to a great degree[34-36]. The efficient separation of electrons and holes in the pNW-580 is further confirmed by the PL spectra. As shown in Fig. S9, the porous Nb_2O_5 nanowires exhibits much lower emission intensity than nonporous nanowires, indicating that the recombination of charge carriers is inhibited in this porous structure. As for the comparison between pNW-580 and pNW-600, the even higher annealing temperature and increased porosity in pNW-600 doesn't bring about better performance than pNW-580 probably due to the reconfiguration of the surface atoms around the enclosed pores during phase transition which leads to the removal of the defects and the mid-gap states. In addition to the increased bandgap and decreased absorption, the lower crystallinity of pNW-600 and inefficient charge separation further exacerbate the sluggish reaction of RhB degradation.

CONCLUSIONS

In summary, nanowires of Nb_2O_5 with enclosed pores were successfully synthesized via hydrothermal process. The porous nanowires synthesized at appropriate temperature display a fairly high photocatalytic activity in the photocatalytic degradation of RhB and hydrogen evolution under both UV and visible-light irradiation and is advantageous over nonporous nanowires of Nb_2O_5 and the commercial photocatalyst. The unique porous nanowire structure of Nb_2O_5 may play the pivotal role in tuning the performance by narrowing the band gap, enhancing the visible light absorption and increasing charge separation efficiency.

We hope the trapped-pore induced photocatalytic enhancement could be further explored and applied to the design of high-performance photocatalysts.

Received xxx 2015; accepted xxx 2015;
Published online xxx 2015

1 Jose R, Thavasi V, and Ramakrishna S. Metal Oxides for Dye - Sensitized Solar Cells. Journal of the American Ceramic Society, 2010, 92: 289-301.
2 Viet AL, Jose R, Reddy MV, et al. Nb_2O_5 Photoelectrodes for Dye-Sensitized Solar Cells: Choice of the Polymorph. Journal of Physical Chemistry C, 2010, 114: 21795-21800.
3 Hota MK, Bera MK, Verma S, et al. Studies on switching mechanisms in Pd-nanodot embedded Nb_2O_5 memristors using scanning tunneling microscopy. Thin Solid Films, 2012, 520: 6648-6652.
4 Graça MPF, Meireles A, Nico C, et al. Nb_2O_5 nanosize powders prepared by sol-gel - Structure, morphology and dielectric properties. Journal of Alloys & Compounds, 2013, 553: 177-182.
5 Ghosh R, Brennaman MK, Uher T, et al. Nanoforest Nb_2O_5 Photoanodes for Dye-Sensitized Solar Cells by Pulsed Laser Deposition. Acs Appl Mater Interfaces, 2011, 3: 3929-3935.
6 Mujawar SH, Inamdar AI, Betty CA, et al. Effect of post annealing treatment on electrochromic properties of spray deposited niobium oxide thin films. Electrochimica Acta, 2007, 52: 4899-4906.
7 Viet AL, Reddy MV, Jose R, et al. Nanostructured Nb_2O_5 Polymorphs by Electrospinning for Rechargeable Lithium Batteries. Journal of Physical Chemistry C, 2010, 114: 664-671.
8 Rani RA, Zoolfakar AS, O'Mullane AP, et al. Thin films and nanostructures of niobium pentoxide: fundamental properties, synthesis methods and applications. Journal of Materials Chemistry A, 2014, 2: 15683-15703.
9 Saupe GB, Zhao Y, Bang J, et al. Evaluation of a new porous titanium-niobium mixed oxide for photocatalytic water decontamination. Microchemical Journal, 2005, 81: 156-162.
10 Lam SM, Sin JC, Satoshi I, et al. Enhanced sunlight photocatalytic performance over Nb_2O_5/ZnO nanorod composites and the mechanism study. Applied Catalysis A General, 2014, 471: 126-135.
11 Zhao W, Zhao W, Zhu G, et al. Black Nb_2O_5 nanorods with improved solar absorption and enhanced photocatalytic activity. Dalton Transactions, 2016, 45: 3888-3894.
12 Yang G, Yan W, Zhang Q, et al. One-dimensional CdS/ZnO core/shell nanofibers via single-spinneret electrospinning: tunable morphology and efficient photocatalytic hydrogen production. Nanoscale, 2013, 5: 12432-9.
13 Sun Z, Liao T, and Kou L. Strategies for designing metal oxide nanostructures. Science China Materials, 2017, 60: 1-24.
14 Tong H, Ouyang S, Bi Y, et al. Nano-photocatalytic Materials: Possibilities and Challenges. Advanced Materials, 2012, 24: 229-251.
15 Han Y, Wu X, Ma Y, et al. Porous SnO_2 nanowire bundles for photocatalyst and Li ion battery applications. Crystengcomm, 2011, 13: 3506-3510.
16 Wang G, Li Z, Li M, et al. Synthesizing Vertical Porous ZnO Nanowires Arrays on Si/ITO Substrate for Enhanced Photocatalysis. Ceramics International, 2017, 44: 1291-1295
17 Zhang M, Ci S, Li H, et al. Highly defective porous CoP nanowire as electrocatalyst for full water splitting. International Journal of Hydrogen Energy, 2017, 42: 29080-29090
18 Li R, Chen S, Lou Z, et al. Fabrication of porous SnO_2 nanowires gas sensors with enhanced sensitivity. Sensors & Actuators B Chemical, 2017, 252: 79-85
19 Li X, Ma Y, Cao G, et al. FeOx@carbon yolk/shell nanowires with tailored void spaces as stable and high-capacity anodes for lithium ion batteries. Journal of Materials Chemistry A, 2016, 4: 12487-12496.
20 Zhou B, Yang S, Wu L, et al. Amorphous Carbon Framework Stabilized SnO_2 Porous Nanowires as High Performance Li-ion Battery Anode Materials. Rsc Advances, 2015, 5: 49926-49932.
21 Zhou B, Yang S, Wu W, et al. Self-assemble SnO_2@TiO_2 porous nanowire–nanosheet heterostructures for enhanced photocatalytic property. CrystEngComm, 2014, 16: 10863-10869.
22 Song J, Li H, Li S, et al. Electrochemical synthesis of MnO_2 porous nanowires for flexible all-solid-state supercapacitor. New Journal of Chemistry, 2017, 41: 3750-3757.
23 Yin J, Li Y, Lv F, et al. NiO/CoN Porous Nanowires as Efficient Bifunctional Catalysts for Zn-Air Batteries. Acs Nano, 2017, 11: 2275-2283.
24 Duan XW, Wang GZ, Wang HQ, et al. Orientable pore-size-distribution of ZnO nanostructures and their superior photocatalytic activity. Crystengcomm, 2010, 12: 2821-2825.
25 Wang Q, Chen G, Zhou C, et al. Sacrificial template method for the synthesis of CdS nanosponges and their photocatalytic properties. Journal of Alloys and Compounds, 2010, 503: 485-489.
26 Lu B, Zhu C, Zhang Z, et al. Preparation of highly porous TiO_2 nanotubes and their catalytic applications. Journal of Materials Chemistry, 2011, 22: 1375-1379.
27 Xu L, Dong B, Wang Y, et al. Electrospinning preparation and room temperature gas sensing properties of porous In_2O_3 nanotubes and nanowires. Sensors & Actuators B Chemical, 2010, 147: 531-538.
28 Dou Z, Cao C, Chen Y, et al. Fabrication of porous Co_3O_4 nanowires with high CO sensing performance at a low operating temperature. Chemical Communications, 2014, 50: 14889-91.
29 Wan J, Sun L, Fan J, et al. Facile synthesis of porous Ag_3PO_4 nanotubes for enhanced photocatalytic activity under visible light. Applied Surface Science, 2015, 355: 615-622.
30 Brayner R and Bozonverduraz F. Niobium pentoxide prepared by soft chemical routes: morphology, structure, defects and quantum size effect. Physical Chemistry Chemical Physics, 2003, 5: 1457-1466.
31 Takizawa T, Watanabe T, and Honda K. Photocatalysis through excitation of adsorbates. 2. A comparative study of Rhodamine B and methylene blue on cadmium sulfide. Journal of Physical Chemistry, 1978, 82: 1391-1396.
32 Wu T, Guangming Liu A, Zhao J, et al. Evidence for H_2O_2 Generation during the TiO2-Assisted Photodegradation of Dyes in Aqueous Dispersions under Visible Light Illumination. International Journal of Gynecological Cancer, 1999, 9: 117–122.
33 Wu T, Guangming Liu A, Zhao J, et al. Photoassisted Degradation of Dye Pollutants. V. Self-Photosensitized Oxidative Transformation of Rhodamine B under Visible Light Irradiation in Aqueous TiO_2 Dispersions. Journal of Physical Chemistry B, 1998, 102: 5845-5851.
34 Pan J, Utama MIB, Zhang Q, et al. Composition - Tunable Vertically Aligned CdS_xSe_{1-x} Nanowire Arrays via van der Waals Epitaxy: Investigation of Optical Properties and Photocatalytic Behavior. Advanced Materials, 2012, 24: 4151-6.
35 Ishibashi KI, Fujishima A, Watanabe T, et al. Quantum yields of active oxidative species formed on TiO_2 photocatalyst. J Photochem Photobiol A Chem. Journal of Photochemistry & Photobiology A Chemistry, 2000, 134: 139-142.
36 Carraway ER, Hoffman AJ, and Hoffmann MR. Photocatalytic oxidation of organic acids on quantum-sized semiconductor colloids. Environmental Science & Technology, 1994, 28: 786-93.

Acknowledgements This work was financial supported by the National Science Foundation of China (No. 51271215 and 21601133) and Sinopec Innovation Scheme (A-381). We gratefully

acknowledge Dr. Xin Sun from Tianjin University of Technology for his help on the HRTEM.

Author contributions Zhang Y designed the experiment; Zhao H, Zhao X, Lin J and Li N performed the experiments; Zhang Y wrote the paper with support from Huo ZY, Zhang M and Hu S. All authors contributed to the general discussion.

Conflict of interest The authors declare that they have no conflict of interest.

Supplementary information supporting data are available in the online version of the paper.

SCIENCE CHINA Materials ARTICLES

Ying Zhang received her BE degree in Shandong University in 1998. She obtained her PhD degree in Chemical Engineering and Technology at China University of Petroleum in 2008. Now she is an associate professor at the College of Chemical Engineering of the China University of Petroleum. Her research expertise is nanomaterials for catalysis, energy storage and conversion.

Miao Zhang received her Ph.D from Institute of Chemistry, Chinese Academy of Science. After her postdoctoral research in Lawrence Berkeley National Laboratory, she is currently a research scientist in Chemical Science Division at LBNL. Her research interests encompass the development of photocatalyst and Operando spectroscopy.

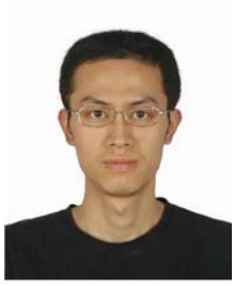

Shi Hu received his BS degree in Nanjing University in 2002 and his PhD degree in Chemistry from Tsinghua University in 2012. After the post-doctoral research in North Carolina State University and Pennsylvania State University, he is now a professor in the department of chemistry of Tianjin University. His research interest is development of new materials and nanostructures for photocatalysis, electrocatalysis and gas sensing.

内嵌孔型窄带隙Nb_2O_5纳米线及其光催化研究

张颖，赵虎，赵小菲，林建楠，李娜，霍子扬，闫子峰，张苗，胡适

[illegible]

[illegible] Nb_2O_5 [illegible]

[illegible]

[1] State Key Laboratory for Heavy Oil Processing, PetroChina, Key Laboratory of Catalysis, China University of Petroleum, Qingdao 266580, China
[2] Department of Chemistry, School of Science, Tianjin Key Laboratory of Molecular Optoelectronic Science, Tianjin University, Tianjin 300072, China.
[3] Queensland Micro- and Nanotechnology Centre, Griffith University, Brisbane 4111, Australia
[4] Chemical Science Division, Department of Chemistry, University of California Berkeley 94720, USA
* Corresponding author (email: rychushi@gmail.com, MZhang@lbl.gov)

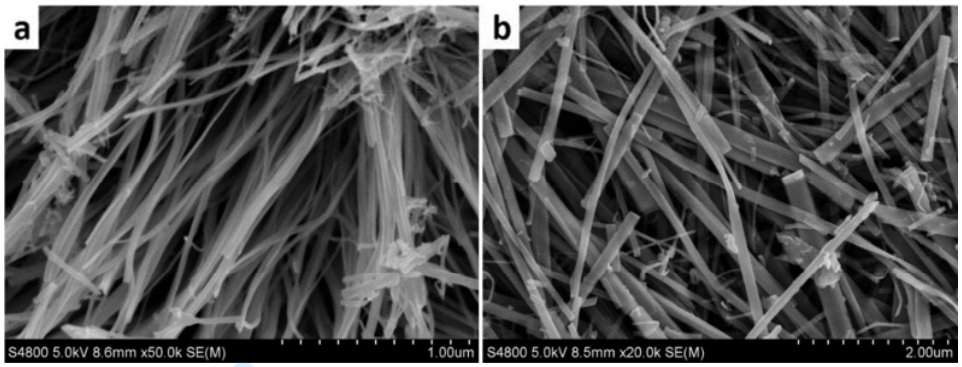
a
b
S4800 5.0kV 8.6mm x50.0k SE(M)
1.00um
S4800 5.0kV 8.5mm x20.0k SE(M)
2.00um

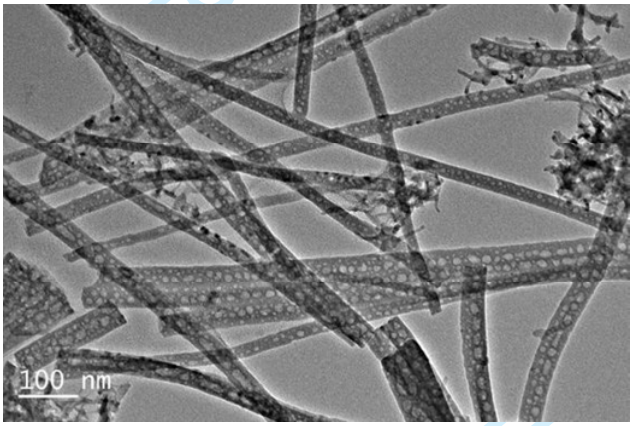
100 nm

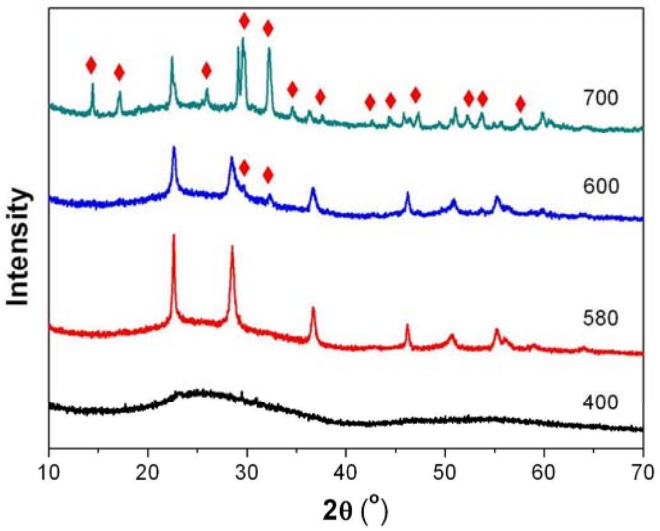
700
600
580
400
Intensity
10
20
30
40
50
60
70
2θ (°)

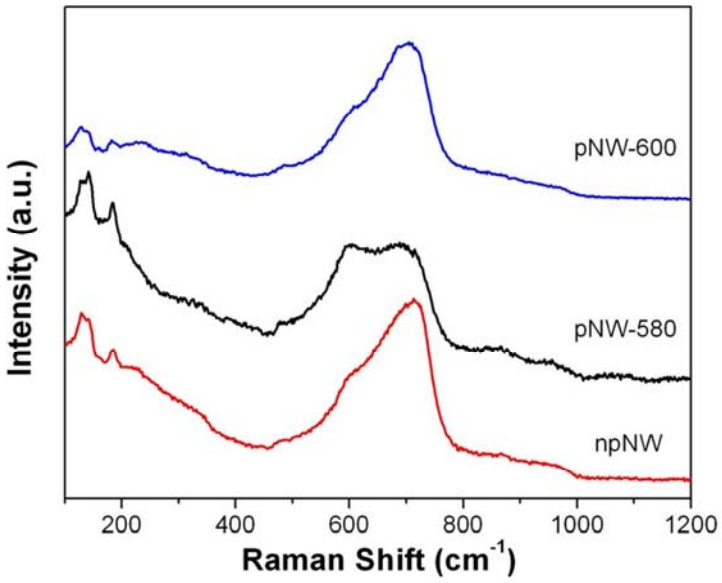
pNW-600
pNW-580
npNW
Intensity (a.u.)
200
400
600
800
1000
1200
Raman Shift (cm-1)

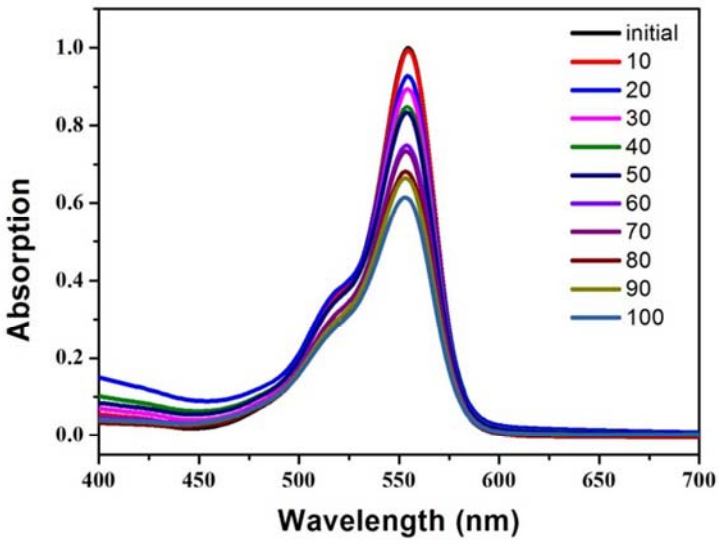
initial
10
20
30
40
50
60
70
80
90
100
Absorption
Wavelength (nm)

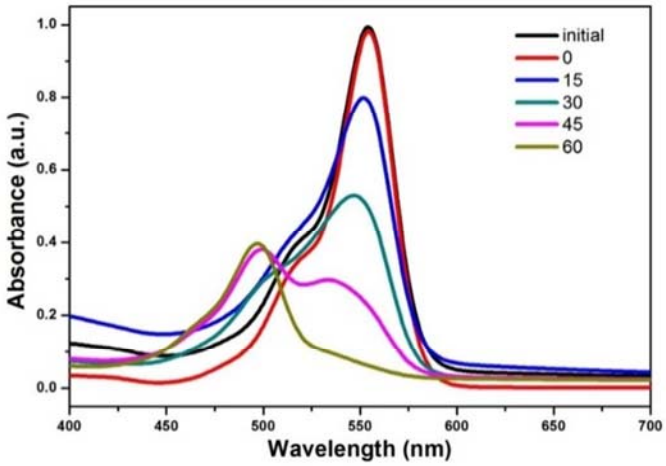
initial
0
15
30
45
60
Absorbance (a.u.)
Wavelength (nm)

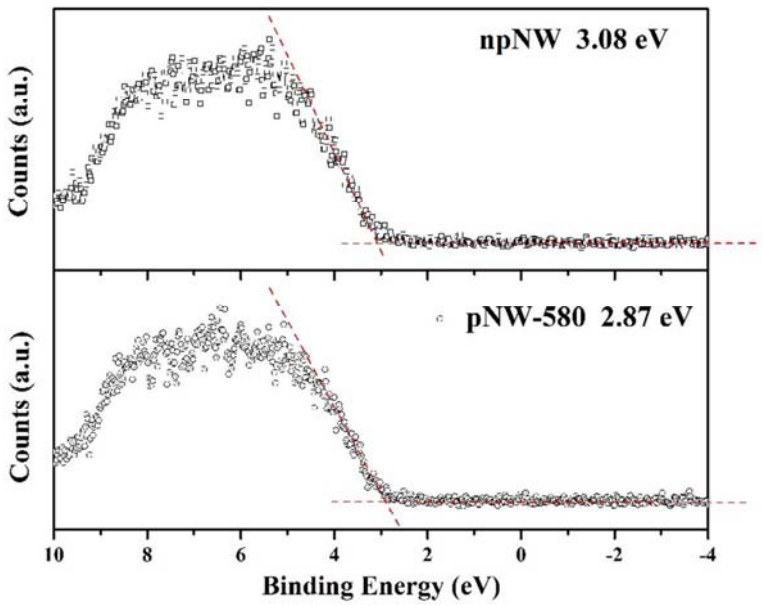
npNW 3.08 eV
pNW-580 2.87 eV
Counts (a.u.)
Counts (a.u.)
10
8
6
4
2
0
-2
-4
Binding Energy (eV)

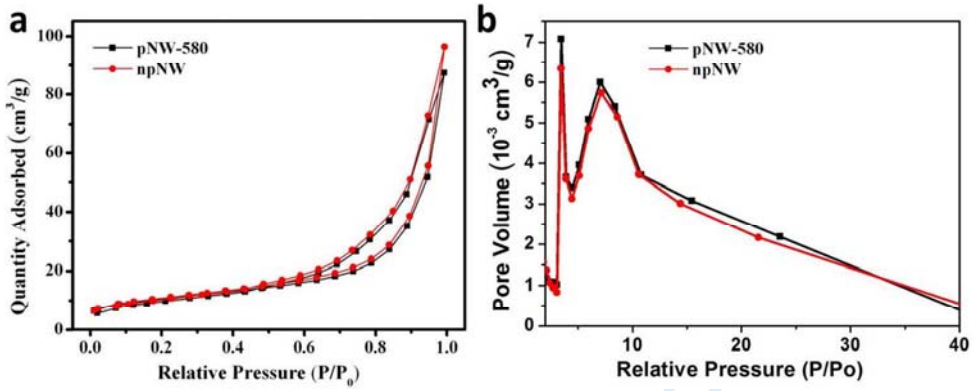
a
pNW-580
npNW
Quantity Adsorbed (cm³/g)
Relative Pressure (P/P0)
b
pNW-580
npNW
Pore Volume (10⁻³ cm³/g)
Relative Pressure (P/Po)